

A New Particle Filter Framework for Bayesian Receiver Autonomous Integrity Monitoring in Urban Environments

Shubh Gupta¹, Grace Xingxin Gao²

¹Department of Electrical Engineering, Stanford University

²Department of Aeronautics & Astronautics, Stanford University

Abstract: Existing urban navigation algorithms employ integrity monitoring (IM) to mitigate the impact of measurement bias errors and determine system availability when estimating the position of a receiver. Many IM techniques, such as receiver autonomous integrity monitoring (RAIM), utilize measurement residuals associated with a single receiver position to provide integrity. However, identifying a single correct receiver position is often challenging in urban environments due to low satellite visibility and multiple measurements with bias errors. To address this, we propose Particle RAIM as a novel framework for robust state estimation and IM using GNSS and odometry measurements. Particle RAIM integrates residual-based RAIM with a particle filter and Gaussian mixture model likelihood to jointly perform state estimation and fault mitigation using a multimodal probability distribution of the receiver state. Our experiments on simulated and real-world data show that Particle RAIM achieves smaller positioning errors as well as smaller probability of false alarm and probability of missed-identification in determining system availability than existing urban localization and IM approaches in challenging environments with a relatively small computation overhead.

Keywords: Particle filter, Receiver Autonomous Integrity Monitoring, Global Navigation Satellite Systems, urban environment, mixture models, Sequential Monte Carlo, Expectation-Maximization.

I. Introduction

Global Navigation Satellite System (GNSS) based navigation in urban environments is subject to various impairments, such as limited satellite visibility, signal attenuation and the multipath effect [1]. Such impairments to GNSS signals result in fewer measurements as compared to open-sky conditions and bias errors, or *faults*, in measurements. Therefore, both accurately estimating the receiver position under these challenging conditions as well as determining the trustworthiness of the said position are of primary concern for navigation safety in urban environments.

Integrity is defined as the measure of trust that can be placed in the correctness of information supplied by a navigation system [2]. Receiver Autonomous Integrity Monitoring (RAIM) algorithms identify and eliminate degraded GNSS measurements using redundant information, and both provide a position estimate that is robust to measurement bias errors as well inform the user when the provided position estimate is unreliable [3]. However, most RAIM techniques have been developed for the aviation domain, and assume good satellite visibility and signal transmission. Therefore, the current state-of-the-art RAIM techniques cannot be directly used in urban environments, which can have multiple contaminated measurements at any given time instant, and therefore insufficient redundancy in measurements.

A. Prior Work

Current RAIM algorithms are typically characterized as either solution-separation or residual-based approaches [4]. Solution-separation RAIM algorithms [5, 6, 7] consider multiple *fault hypotheses* associated with different subsets

of the available measurement set. The algorithm then computes test statistics measuring the separation between the position solutions from the different fault hypotheses and the all-in-view solution to discard erroneous measurements and assess whether the obtained position solution is reliable, or *available*. However, specifying the different fault hypotheses is computationally intensive even for a moderate number of measurements, since the number of possible measurement subsets is combinatorial in the number of measurements and the number of faults considered [4]. Recent work [8] proposed grouping different fault hypotheses to reduce computation in solution-separation RAIM algorithms. However, the approach is challenging to scale for urban environments where multiple measurements might have bias errors.

On the other hand, residual-based RAIM algorithms [9, 10, 11] treat position estimation and measurement fault exclusion as an iterative process, where all the available measurements are initially used to compute a position solution. The obtained solution is then used to compute *residuals* for each measurement as well as a chi-squared distribution based test statistic. Measurements with the largest residuals are then eliminated from the set of all measurements till the test statistic falls below a specified threshold. A new position solution is then computed using the reduced set of measurements and the process is repeated until no measurements can be removed. However, residual-based RAIM is sensitive to factors such as the fraction of measurements with bias errors present in the complete measurement set. For instance, if a large fraction of obtained GNSS measurements contains bias errors, the initial position fix using these measurements could be significantly off from the true position. Thus, excluding measurements based on the residuals computed using this position fix can result in incorrect exclusions, leading to further positioning errors in subsequent position fixes using the remaining measurements.

Furthermore, many existing RAIM algorithms are *snapshot*, i.e., they estimate positions and determine integrity for each time instant independently [12, 13, 5]. Since snapshot algorithms typically only use GNSS measurements, they require a large number of measurements to compute a position solution and determine the integrity of the system. For example, at least four measurements are required to be available at each time instant for computing a state solution consisting of horizontal position and receiver clock bias as well as for determining the integrity of the system [3], which is a restrictive requirement in urban environments.

Sequential integrity monitoring (SIM) algorithms combine filtering methods including, in some systems, measurements from inertial sensors with RAIM to allow information exchange over different time instants. Grosch *et al.* [14] combine Kalman filter with snapshot RAIM approaches for railway applications. Hewitson *et al.* [15] and Li *et al.* [16] combine extended Kalman filter (EKF) with RAIM to detect step and ascending ramp fault profiles in GNSS measurements. Additionally, Li *et al.* [16] derive protection levels using mean position error bound for integrity monitoring. Tanil *et al.* [17] utilize the innovation sequence of a Kalman filter for sequential integrity monitoring. Although Kalman filter-based methods are useful for estimating the receiver position and monitoring integrity in scenarios containing few measurements with bias errors, these techniques have limited positioning performance in urban environments. This is because these techniques approximate the probability distribution of receiver state and the measurement error probability at a time instant using a Gaussian distribution, while the probability of measurement errors in urban environments can be significantly non-Gaussian due to multipath and systematic receiver errors [1].

Particle filters have been utilized in [18, 19] to track the receiver state using GPS measurements in challenging scenarios with non-Gaussian measurement errors. A particle filter approximates the receiver state probability distribution using a finite set of samples (particles), and can model non-Gaussian probability distributions with multiple modes [20]. For SIM using particle filters, [19, 21, 22, 23] construct multiple filters associated with different subsets of the available measurement set, and detect faulty measurement using the logarithmic likelihood ratio test between the particles tracked by the constructed filters. However, this approach is computationally demanding because a large number of filters need to be constructed to detect and isolate faulty measurements. Thus, this approach is difficult to scale for multiple erroneous measurements in the set of available GNSS measurements. [24, 25, 26] propose techniques to identify and exclude multipath-degraded or non line-of-sight (NLOS) GNSS measurements using a particle filter and a 3D model of the environment. However, procuring and maintaining such a 3D model of the environment on a large scale is difficult.

In another line of work, Pesonen [27] propose a fully Bayesian framework for receiver autonomous integrity monitoring in urban environments. The framework is described for a variety of Bayesian filters which operate

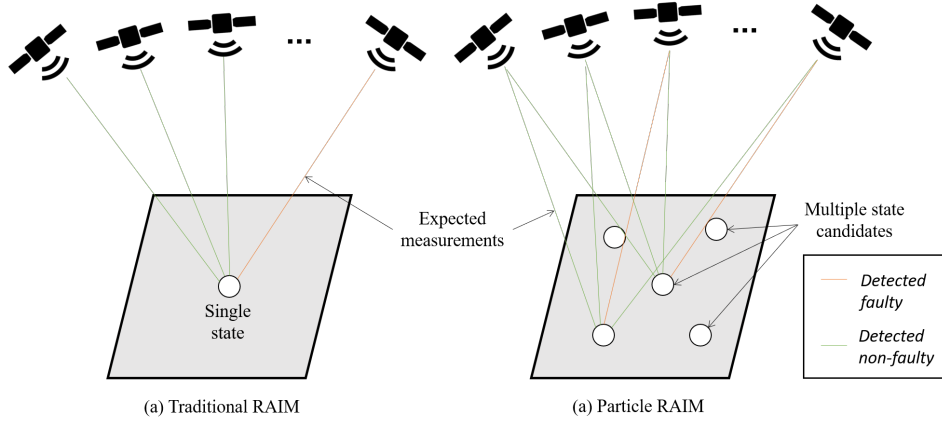


Figure 1: Comparison between traditional RAIM algorithms (left) and proposed Particle RAIM algorithm (right). Traditional RAIM algorithms estimate a single position using a single subset of measurements detected as non-faulty. Particle RAIM simultaneously considers multiple candidate states within a particle filter probability distribution and measurement subsets to robustly capture the probability distribution of the state in the presence of ambiguous measurements.

Traditional RAIM	Particle RAIM
Computes a single state estimate and covariance	Computes a multimodal probability distribution of the state in the form of particles
Estimates the state and mitigates measurement faults separately	Jointly computes the probability distribution of the state and mitigates measurement faults in a single Bayesian framework
A single final hypothesis of measurement faults is considered	Multiple measurement fault hypotheses are considered in computing weights for different particles

Table 1: Comparison between traditional RAIM and the proposed Particle RAIM algorithm.

on a state-space comprising of both receiver position, velocity and time parameters as well as multipath bias indicators for all the available GNSS measurements. Using the probability distribution of the state estimated by filters, measures of accuracy and integrity risk are derived and compared against prespecified requirements for determining the system availability. The approach proposed in [27] monitors integrity directly in the position domain, such that the proposed integrity monitor declares the system 'available' if the position error is within a specified alarm limit, and 'unavailable' otherwise. In our approach, we adopt a similar framework for integrity monitoring that determines the system availability through measures of accuracy and integrity risk derived using Bayesian principles.

B. Our Approach

In this paper, we build upon our prior work on the Particle RAIM algorithm [28] to address the challenges towards providing safe and robust localization in urban environments using GNSS and odometry measurements. Particle RAIM jointly addresses the tasks of state estimation and fault mitigation within a Bayesian framework. A position solution estimated by relying on any single subset of GNSS measurements, such as in [9, 5], can be erroneous when a large fraction of the measurements contain faults. Therefore, our Bayesian framework simultaneously considers multiple positions supported by different groups of GNSS measurements in the form of a multimodal probability distribution of the state represented using particles (Fig. 1, Table 1). Therefore, in scenarios where a correct state estimate cannot be clearly identified, we assign similar probabilities to all different position solutions that are likely when different subsets of the available measurements are considered. We evaluate the probability

associated with each position using a Gaussian mixture model (GMM) likelihood [29] over the GNSS measurements. The GMM likelihood is characterized by a weighted sum of multiple probability distribution components. Each component in our GMM represents the conditional probability distribution of observing a single GNSS measurement from a position. The weight coefficients in the GMM are derived from the particle distribution at each time instant, and are determined at runtime. The number of GMM components at a time equals the number of available measurements. Our GMM likelihood assigns high probability to positions that are supported by measurements with high weight coefficients. Therefore, for fault mitigation, Particle RAIM assigns low values to the weight coefficients of GMM components corresponding to faulty GNSS measurements.

Similar to prior work in particle filter-based sequential integrity monitoring, we leverage the correlation in measurements across time instants by (1) adopting a particle filter-based approach [20] and (2) using odometry measurements from an inertial measurement unit (IMU). Since our algorithm leverages information from measurements seen in previous time instants, it is less sensitive to the number of measurements at a time instant than snapshot approaches. The probability distribution of the receiver state is modeled as weighted particles in a particle filter, where the weights are determined along with the GMM likelihood weight coefficients. To jointly estimate the particle weights and GMM weight coefficients, we develop an iterative scheme based on the expectation-maximization (EM) algorithm [30]. Inspired by the residual-based RAIM methodology [9], our algorithm starts from initial values of the particle weights and GMM weight coefficients, and then repeatedly refines the particle weights and GMM weight coefficients using GNSS measurements to compute a probability distribution of the state and a state estimate that is robust to measurement faults. To determine the system availability, we follow a similar methodology as [27] and compute measures of integrity risk and accuracy. The approach to compute integrity risk in [27] uses the particle filter probability distribution, which can fail in approximating the parts of the probability distributions that are distant from the state estimate [31]. Therefore, we develop an alternative approach for computing integrity risk using the GMM likelihood. We declare our system available if the computed integrity risk and accuracy meet prespecified requirements.

Particle RAIM provides several advantages over prior work. Our algorithm achieves smaller state estimation errors and fewer false alarms and missed identifications in determining system availability as compared to existing approaches in urban environments with multiple measurement faults. Unlike the existing particle filter-based SIM approaches that exhibit a combinatorial increase in required computation with larger number of measurements and measurement faults, our approach scales linearly in computation with the number of measurements. The linear scaling of computation in Particle RAIM is due to the iterative approach for directly mitigating multiple faults instead of considering different subsets of measurements as is done in existing approaches. Unlike the state estimation techniques proposed in Bayesian RAIM [27], our approach does not require a known transition model over measurement faults across different time instants. Furthermore, our approach for computing integrity risk explicitly considers the multimodal and heavy-tailed nature of the position probability distribution through the GMM likelihood, unlike the particle-based approach described in [27].

The contributions of our work are five fold:

1. We propose a novel Bayesian framework for robust state estimation and integrity monitoring using GNSS and odometry measurements in urban scenarios, with possibly multiple faulty GNSS measurements and limited satellite visibility. Our framework integrates the particle filter algorithm [20] with the residual-based RAIM methodology to efficiently construct a probability distribution of the state such that the high probability positions are supported by combinations of different GNSS measurements at a time instant.
2. We develop a novel measurement likelihood model based on the Gaussian mixture model [29], whose weight coefficients are determined at runtime, for evaluating the probability associated with receiver position in urban environments with multiple faulty GNSS measurements. Each component in the likelihood model corresponds to a single measurement and is associated with a weight coefficient. We design an iterative scheme based on the EM algorithm [30] to compute the weight coefficients jointly with a probability distribution of the state, such that the impact of measurements bias errors on the computed state probability distribution is minimal.
3. We design a computationally efficient algorithm for jointly estimating the state probability distribution and mitigating GNSS measurement faults that scales linearly in computation with the number of measurements.

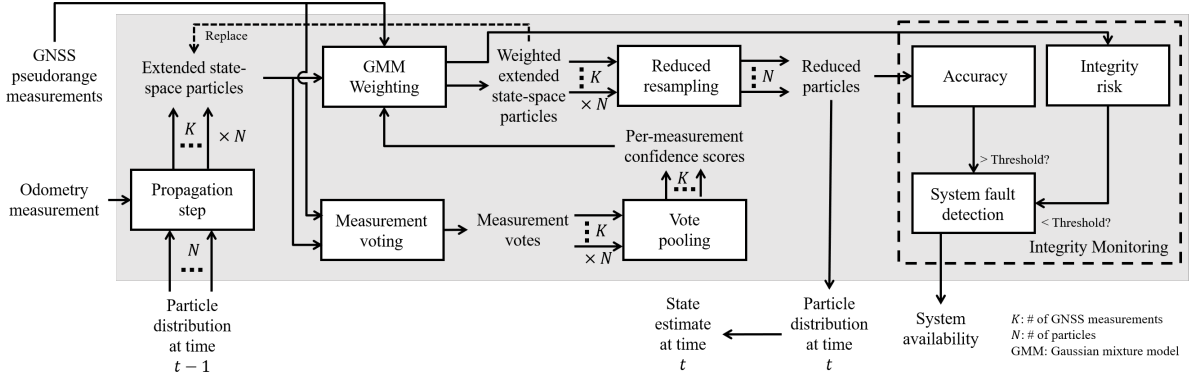


Figure 2: Architecture of Particle RAIM algorithm. Probability distribution of the vehicle state is estimated as a set of weighted particles in a particle filter. Propagation step generates replicas of each particle for all GNSS measurements, denoted as extended state-space particles, and propagates them using an odometry-based motion model. For each extended state-space particle and its associated GNSS measurement, Measurement voting step computes the probability of observing the measurement residual under a chi-squared distribution, denoted as a measurement vote. Vote pooling step combines the votes obtained across particles to compute weighting coefficients, or confidence scores, in a GMM measurement likelihood model where each confidence score is associated with a single measurement probability component in the GMM. Then, a GMM measurement likelihood is constructed using the confidence scores and weights associated with all extended state-space particles are updated. The process is then repeated for a fixed number of iterations using the new extended state-space particles. Finally, the particles are resampled and reduced to the original size to obtain the new particle distribution as well as the state estimate. For integrity monitoring using the state estimate, availability of the system is determined by computing measures for integrity risk as well as accuracy and comparing them against prespecified thresholds.

Our algorithm uses an iterative approach and particle filter probability distribution to mitigate the impact of faulty measurements on state estimation, instead of considering different subsets of measurements individually.

4. For integrity monitoring and detecting system-level failures, we compute integrity risk by approximating the integral over our GMM likelihood for positions within a fixed radius of the state estimate. Unlike existing integrity monitoring approaches that use particle filter distribution, our approach explicitly considers the parts of the state probability distribution that are distant from the state estimate.
5. We have validated our approach on real-world data as well as simulated scenarios with various noise profiles imitating urban environments. We compared our approach with existing sequential integrity monitoring techniques and demonstrated that our algorithm results in smaller positioning errors as well as smaller probability of false alarm and probability of missed-identification in determining system availability than the compared approaches in challenging scenarios with multiple faulty measurements.

The rest of the paper is organized as follows: Section II discusses the Particle RAIM algorithm in detail. In Section III, we discuss the validation experiments for our approach on both simulated and real-world data and compare it with existing techniques. Section IV summarizes our work.

II. Particle RAIM Framework

The architecture of the Particle RAIM algorithm is outlined in Fig. 2. At each time instant, Particle RAIM takes as input the GNSS and IMU measurements, as well as the particle distribution computed at the previous time instant. Particle RAIM operates on the extended state-space of particles, which consists of the receiver state as well as an integer denoting one GNSS measurement associated with the particle that is assigned when the particle is created. The weighted particles from the probability distribution at the previous time instant are converted to the extended state-space particles in the propagation step by creating replicas of each particle for all GNSS measurements. Each extended state-space particle is then propagated using a motion model based on odometry

measurements. To update the weights of the extended state-space particles using GNSS measurements, we then develop a three-step iterative approach. In the measurement voting step, we compute probabilistic votes from the extended state-space particles to their associated measurements using the chi-squared probability distribution [32]. The measurement votes are then combined in the vote pooling step to obtain the GMM weight coefficients, or confidence scores, for each GMM probability component associated with a GNSS measurement. Using the GMM constructed with the obtained confidence scores, we update the weights of each extended state-space particle. We then repeat the process using the new extended state-space particles for a fixed number of iterations, or until convergence. The reduced resampling step then generates a new set of particles with equal weights and reduces the extended state-space of the particles to receiver state-space. For integrity monitoring, we first compute the measures for accuracy and integrity risk using the particles and the GMM likelihood. Then, we compare the obtained accuracy and integrity risk against prespecified requirements to determine the availability of the system. While the approach presented in this paper focuses on GNSS and odometry measurements, our approach can be generalized to incorporate measurements from other sensors, such as camera or LiDAR, in computing the particle weights.

A. Problem Setup

Consider a vehicle navigating in an urban environment using GNSS and odometry measurements. We denote the true state vector of the vehicle at time t as x_t , and the overall trajectory as $\{x_t\}_{t=1}^T$, where T denotes the total duration of the vehicle's trajectory. For generality, we do not restrict the state vector x_t to have a specific form and instead assume that it consists of combinations of various quantities such as the vehicle's position coordinates, heading angles, receiver clock errors, linear velocities, and yaw rates. The k th GNSS pseudorange measurement acquired at time t is denoted by the scalar value $\rho_t^{(k)}$. At time t , the vehicle acquires a set of K_t GNSS pseudorange measurements $M_t = \{\rho_t^{(k)}\}_{k=1}^{K_t}$ and odometry measurement u_t . The probability distribution π_t of the vehicle state is approximated by a particle filter as,

$$\pi_t = P(x_t|x_{t-1}, M_t, u_t) \approx \hat{\pi}_t = \sum_{i=1}^N w_t^{(i)} \delta(x = x_t^{(i)}), \quad (1)$$

where

$\hat{\pi}_t$ denotes the approximate state probability distribution represented using particles;

$x_t^{(i)}$ denotes the state of the i th particle;

$w_t^{(i)}$ denotes the weight of the i th particle such that $\sum_{i=1}^N w_t^{(i)} = 1$;

$\delta(x = x_t)$ denotes the Dirac delta function [33] that assumes the value of zero everywhere except x_t ;

N is the total number of particles.

The expression for π_t assumes the Markov property among state variables (x_1, \dots, x_t) , which means that x_t depends on the past states and measurements $(x_1, \dots, x_{t-1}, M_1, \dots, M_{t-1}, u_1, \dots, u_{t-1})$ only through x_{t-1} . Hence, the conditional probabilities $P(x_t|x_{t-1}, M_t, u_t)$ and $P(x_t|x_1, \dots, x_{t-1}, M_1, \dots, M_t, u_t)$ are equivalent. The particle weights $\{w_t^{(i)}\}_{i=1}^N$ are initialized uniformly to be N^{-1} . Following the methodology in standard filtering algorithms [34] and applying Bayes theorem with independence assumptions on M_t, u_t , the probability distribution can be factorized as,

$$\begin{aligned} P(x_t|x_{t-1}, M_t, u_t) &\propto P(M_t|x_t, x_{t-1}, u_t) \cdot P(x_t|x_{t-1}, u_t) \\ &\propto \underbrace{P(M_t|x_t)}_{L_t(x_t)} \cdot \underbrace{P(x_t|x_{t-1}, u_t)}_{\hat{\pi}_t}, \end{aligned} \quad (2)$$

where

$L_t(x_t)$ can be interpreted as the likelihood of receiving the set of measurements M_t at time t from state x_t ;

$\tilde{\pi}_t$ is the propagation term which denotes the predicted probability distribution at time t that is approximated using the particle probability distribution at previous time $\hat{\pi}_{t-1}$ and odometry measurement u_t .

In Particle RAIM, we consider the joint tasks of state estimation and fault mitigation using an extended state-space (x, χ) of particles, where $\chi = k \in \{1, \dots, K_t\}$ denotes an integer corresponding to the k th GNSS measurement in the measurement set M_t . The value of χ is assigned to each extended state-space particle at the time of its creation in the propagation step, and remains fixed until the state-space of the particles is reduced to just the vehicle state-space in the reduced resampling step. The extended state-space particles are used in the iterative weighting step to determine the weight coefficients in the GMM likelihood as well as to compute the particle weights.

We next provide details about each algorithmic step in Particle RAIM.

B. Propagation Step

The propagation term is approximated by applying a Markov chain transition using known system dynamics and odometry measurement u_t on the extended state-space particle distribution computed from the particle distribution $\hat{\pi}_{t-1}$ at the previous timestep $t-1$. For computing the extended state-space particles from $\hat{\pi}_{t-1}$, we first generate uniformly weighted K_t copies of each particle $x_{t-1}^{(i)}$, each corresponding to a different value of $\chi = \{1, \dots, K_t\}$. We then propagate the extended state-space particles $(x, \chi)_{t-1}^{(i)}$ via the state dynamics to get the propagation term,

$$x_t^{(i, \chi)} = f(x_{t-1}^{(i)}, u_t) \quad \forall \chi = \{1, \dots, K_t\}, \quad (3)$$

$$\tilde{\pi}_t^{(i)} = \sum_{k=1}^{K_t} K_t^{-1} \delta(x = \tilde{x}_t^{(i, \chi=k)}), \quad (4)$$

$$\tilde{\pi}_t \approx \sum_{i=1}^N w_{t-1}^{(i)} \tilde{\pi}_t^{(i)}, \quad (5)$$

where

$f(x, u)$ is the function to propagate state x using odometry u based on system dynamics. The stochasticity in propagation is controlled by the propagation noise std. deviation σ_f ;

$x_t^{(i, \chi=k)}$ denotes an extended state-space particle associated with measurement k , and is constructed by propagating the i th particle;

$\tilde{\pi}_t^{(i)}$ denotes the particle distribution consisting of K_t propagated equally-weighted replicas of i th particle.

Next, we compute the measurement likelihood model and update the weights associated with each particle in the weighting step.

C. Iterative Weighting Step

In standard filtering schemes, the measurement likelihood is modeled by assuming independence between measurements as well as correctness of all measurements [34],

$$L_t(x_t) = \prod_{k=0}^{K_t} P(\rho_t^{(k)} | x_t) \quad (6)$$

Existing filtering algorithms for GNSS-based navigation [35, 27, 36] model the probability $P(\rho_t^{(k)} | x_t)$ associated with the k th measurement at time t for x_t as a Gaussian distribution. The mean parameter of the distribution $\hat{\rho}_{x_t}^k$ is set as the expected value of the k th pseudorange measurement from x_t assuming known satellite position, and variance $\sigma_{x_t}^k$ is based on Dilution of Precision (DOP) [37] or is empirically computed. The overall measurement likelihood hence becomes,

$$L_t(x_t) = \prod_{k=0}^{K_t} \mathcal{N}(\rho_t^{(k)} | \hat{\rho}_{x_t}^k, \sigma_{x_t}^k), \quad (7)$$

However, the above mentioned likelihood model inherently assumes a unimodal probability distribution of x_t , and therefore, has a tendency to over simplify in presence of faults in multiple GNSS measurements. For example, a large bias in one measurement, which is common in a multipath degraded environment, may severely reduce the likelihood of a particle even if other measurements support it. Therefore, the likelihood needs to be modeled so that fault in one measurement does not have a dominating effect on the overall measurement likelihood. Additionally, different subsets of measurements can support different regions in the position space and must be modeled as such. Hence, we model the likelihood instead as a Gaussian mixture model (GMM) which has additive contributions of each measurement towards the likelihood unlike the multiplication of individual likelihoods in the former model. Each measurement component in the GMM likelihood is associated with a weight, or *confidence score*, which controls the amount of impact that component has on the overall likelihood. Given a few faulty measurements, an assignment of low confidence scores to their components in the GMM would lower the impact that faulty measurements have on the computed particle weights. The mixture model based likelihood is expressed as,

$$L_t(x_t) = \sum_{k=1}^{K_t} \gamma_k \mathcal{N}(\rho_t^{(k)} | \hat{\rho}_{x_t}^k, \sigma_{x_t}^k) \quad \text{s.t.} \quad \sum_{k=1}^{K_t} \gamma_k = 1, \quad (8)$$

where

γ_k is the confidence score associated with k th measurement. γ_k scales the individual probability distribution components to enforce a unit integral for the probability distribution.

The measurement component for the k th measurement in the GMM assigns similar probabilities to all the positions x_t which generate expected pseudorange measurement values $\hat{\rho}_{x_t}^k$ that are similar to each other. In the particle distribution, a large weight can be assigned to a particle through the GMM likelihood in multiple scenarios. For instance, a high value of particle weight can be computed when a few measurement components with high confidence scores support the particle, or alternatively the particle is supported by multiple measurement components with low confidence scores. Therefore, GMM induces a multi-modal probability distribution over the state, with peaks at positions supported by different subsets of component measurements. Note, that the probability distribution of the state x_t using GMM is multimodal for any configuration of the confidence scores, if the individual measurement components disagree with each other. The values of confidence scores, however, decides the relative confidence between the modes, i.e., for the same values of standard deviation, the mode of the component with higher confidence score has a higher probability value associated with it [29].

Using the proposed GMM likelihood, we jointly determine the values for the measurement confidence scores $\{\gamma_k\}_{k=1}^{K_t}$ and particle weights $\{w_t^{(i)}\}_{i=1}^N$ using a three-step iterative approach. Our approach is based on the EM algorithm for GMM [38] and consists of the measurement voting, vote pooling and GMM weighting steps.

Measurement voting Since we do not assume any prior knowledge about measurement faults, we uniformly initialize the value of γ_k with K_t^{-1} for all values of $k \in \{1, \dots, K_t\}$. The initial value of extended state-space particle weights $\{w_t^{(i, \chi=k)}\}_{i=1}^N$ is set using the previous time instant weights as,

$$w_t^{(i, \chi=k)} = K_t^{-1} \cdot w_{t-1}^{(i)} \quad \forall i \in 1, \dots, N, k \in 1, \dots, K_t. \quad (9)$$

Since the particle weights $\{w_t^{(i)}\}_{i=1}^N$ and confidence scores $\{\gamma_k\}_{k=1}^{K_t}$ are interdependent on each other, we cannot obtain a closed form mathematical expression for their updated values. Therefore, we introduce a set of random variables $\{V^k\}_{k=1}^{K_t}$, referred to as *votes*, to indirectly compute the updates for both particle weights $\{w_t^{(i)}\}_{i=1}^N$ and confidence scores $\{\gamma_k\}_{k=1}^{K_t}$. The vote random variable V^k denotes the confidence associated with the k th measurement given a state x_t . Note that the vote random variable V^k differs from the confidence score γ_k since it also depends on the state random variable x_t . Using the initial values of particle weights $\{w_t^{(i)}\}_{i=1}^N$ and measurement confidence scores $\{\gamma_k\}_{k=1}^{K_t}$, we first compute a probability distribution of the vote random variables $\{V^k\}_{k=1}^{K_t}$. Then, we use the vote random variables $\{V^k\}_{k=1}^{K_t}$ to compute the updated value of particle weights $\{w_t^{(i)}\}_{i=1}^N$ and measurement confidence scores $\{\gamma_k\}_{k=1}^{K_t}$. This is similar to the expectation and maximization steps in the EM algorithm [39], where latent random variables are used to compute indirect updates for the parameters. We model the probability distribution of vote random variables $\{V^k\}_{k=1}^{K_t}$ as a finite-sample set of votes $\{v_i^k\}_{i=1, k=1}^{N, K_t}$,

which is computed using the particle distribution $\tilde{\pi}_t$. For each particle $x_t^{(i,\chi)}$ in $\tilde{\pi}_t$, we compute a vote v_i^k for the measurement corresponding to its extended state-space variable χ using the normalized residual r_i^k between the measurement ρ_t^k and expected measurement $\hat{\rho}_{x_t^{(i,\chi=k)}}^k$ from particle $x_t^{(i,\chi=k)}$,

$$r_i^k = \frac{\rho_t^{(k)} - \hat{\rho}_{x_t^{(i,\chi=k)}}^k}{\sqrt{\sigma_{x_t^{(i,\chi=k)}}^k}}. \quad (10)$$

To compute the vote v_i^k , we leverage the chi-squared distribution, similar to traditional residual-based RAIM techniques [9]. We assume that the squared value of the normalized residual r_i^k from i th particle to the satellite associated with k th measurement is distributed according to the chi-squared distribution with a single degree of freedom, or equivalently, square of the standard Gaussian distribution [32],

$$v_i^k = P_{\mathcal{N}^2(0,1)}\left(\left(r_i^k\right)^2\right), \quad (11)$$

where

$P_{\mathcal{N}^2(0,1)}(\cdot)$ denotes the probability density function under square of standard Gaussian distribution [32].

The chi-squared distribution has a sharper curve than the Gaussian distribution, and hence assigns smaller probability value to large residuals than the Gaussian distribution. This is a desirable property in computing the votes, since the difference in the votes computed for different measurements are more evident.

Vote pooling In the second step, the votes cast by each particle are normalized and pooled to compute the value of γ_k for each measurement. Similar to the maximization step in the EM algorithm [39], we write an expression for the total empirical probability π_t^{tot} at time t of measurements M_t using votes $\{v_i^k\}_{i=1, k=1}^{N, K_t}$ and confidence scores $\{\gamma_k\}_{k=1}^{K_t}$ as,

$$\pi_t^{tot} = \sum_{i=1}^N \sum_{k=1}^{K_t} \gamma_k w_t^{(i,\chi=k)} v_i^k. \quad (12)$$

We maximize π_t^{tot} with respect to $\{\gamma_k\}_{k=1}^{K_t}$ and the constraint $\sum_{k=1}^{K_t} \gamma_k = 1$ to obtain the update rule for vote pooling,

$$\gamma_k = \frac{\sum_{i=1}^N w_t^{(i,\chi=k)} v_i^k}{\sum_{i=1}^N \sum_{k'=1}^{K_t} w_t^{(i,\chi=k')} v_i^{k'}}. \quad (13)$$

The update rule can intuitively be seen as assigning the empirical probability to each γ_k according to the weighted votes.

GMM weighting Using the computed confidence scores $\{\gamma_k\}_{k=1}^{K_t}$, we then update the weights of each extended state-space particle. Given a measurement likelihood model, implementing the particle filter on a machine with finite precision of storing floating point numbers may lead to numerical instability. A commonly used way to avoid finite precision errors is by performing the weighing in the log scale, since a larger variation of weights can be represented with the same number of available bits of information. The weights of the multiplicative likelihood model can be readily converted to a sum of log-likelihoods of individual terms. However, the GMM likelihood is “blocked” by a summation inside the log,

$$\log L_t(x_t) = \log P(M_t|x_t) = \log \left(\sum_{k=1}^{K_t} \gamma_k \cdot \mathcal{N}(\rho_t^{(k)} | \hat{\rho}_{x_t}^k, \sigma_{x_t}^k) \right). \quad (14)$$

Therefore, we consider an extended state-space that includes measurement association variable χ described in previous sections. Hence, the likelihood with respect to the extended state-space is rewritten as,

$$P(M_t|x_t, \chi = k) = \gamma_k \cdot \mathcal{N}(\rho_t^{(k)} | \hat{\rho}_{x_t}^k, \sigma_{x_t}^k). \quad (15)$$

Using simple manipulation, the measurement likelihood can now be equivalently written as a Categorical distribution likelihood [39],

$$P(M_t|x_t, \chi) = \prod_{k=1}^{K_t} (\gamma_k \cdot \mathcal{N}(\rho_t^{(k)} | \hat{\rho}_{x_t}^k, \sigma_{x_t}^k))^{\mathbb{I}[\chi=k]} \quad \text{s.t.} \quad \sum_{k=1}^{K_t} \gamma_k = 1, \quad (16)$$

where

$\mathbb{I}[\cdot]$ denotes the indicator function which is 1 if the condition in its argument is true and zero otherwise.

With this formulation, we take the log of the above expression to obtain the measurement log-likelihood,

$$\log L_t(x_t) = \log P(M_t|x_t) = \sum_{k=1}^{K_t} \mathbb{I}[\chi = k] \left(\log \gamma_k + \log \mathcal{N}(\rho_t^{(k)} | \hat{\rho}_{x_t}^k, \sigma_{x_t}^k) \right) \quad \text{s.t.} \quad \sum_{k=1}^{K_t} \gamma_k = 1. \quad (17)$$

We use the log likelihood derived above to compute the new weights $\{w_t^{(i, \chi=k)}\}_{i=1, k=1}^{N, K_t}$ for each particle in a stable manner,

$$l_k^{(i)} = \log L_t(x_t^{(i, \chi=k)}) - \max_i \left(\log L_t(x_t^{(i, \chi=k)}) \right), \quad (18)$$

$$w_t^{(i, \chi=k)} = \frac{\exp \left(l_k^{(i)} \right)}{\sum_{i=1}^N \exp \left(l_k^{(i)} \right)}. \quad (19)$$

D. Reduced Resampling Step

Resampling is a commonly used technique in particle filters to avoid the problem of particle degeneracy [20]. It achieves this by redistributing particles such that more particles are present in regions of higher importance. Resampling is typically performed via a sequential importance resampling (SIR) procedure [40], where the weights of particles form a categorical distribution from which new particles are sampled. Many advanced resampling schemes, such as KL Divergence based resampling [41], genetic resampling [22], or resampling using chaos theory [23], have been used in particle filter algorithms for GNSS-based navigation. However, these methods are computationally demanding and hence are not explored in this work.

In Particle RAIM, we use the SIR procedure with a modification, where the $N \times K_t$ weighted extended state-space particles are reduced to the original number of particles N with equal weights,

$$\{x_t^{(i)}\}_{i=1}^N \leftarrow \text{SIR} \left(\{(x)_t^{(i, \chi=k)}, w_t^{(i, \chi=k)}\}_{i=1, k=1}^{N, K_t} \right), \quad (20)$$

where

$\text{SIR}(\cdot)$ is the SIR procedure [40] that resamples from the distribution of weighted extended space particles.

The mean state estimate \hat{x}_t denotes the state solution from the algorithm, and is computed as $\hat{x}_t = \sum_{i=1}^N w_t^{(i)} x_t^{(i)}$.

E. Integrity Monitoring

Few approaches have addressed integrity monitoring in scenarios where a non-Gaussian probability distribution of state is available. Pesonen [27] propose a general framework for integrity monitoring for a variety of filtering algorithms and associated probability distributions of state. For probability distribution π_t of state given by a filtering algorithm, measures of integrity risk P_I and accuracy r_A are computed and compared against predefined thresholds to determine the availability of the system.

In Particle RAIM, we develop a Bayesian framework for integrity monitoring similar to [27]. At each time instant, the integrity monitor calculates measures of integrity risk P_I and accuracy r_A , which are derived later in the section. The integrity monitor then compares the integrity risk P_I and accuracy r_A against prespecified reference values to detect whether the positioning error between the Particle RAIM state estimate and the ground truth position exceeds a specified alarm limit. Following the Stanford-ESA integrity diagram [42], we refer to such events as hazardous operations. If hazardous operations are detected, the integrity monitor declares the system as unavailable.

Integrity risk is defined as the probability that the position error at a time instant is greater than a specified alarm limit (AL). In [27], separate particle filter distributions are tracked for different instances of the measurement fault indicator vector. Hence, integrity risk P_I in [27] is computed by combining the particle filter probability distributions across different measurement fault indicators,

$$P_I \approx \hat{P}_I = 1 - \sum_{j=1}^{2^{K_t}} \sum_{i \in \Omega_j} w_t^{(i,j)}, \quad (21)$$

where

\hat{P}_I is the estimated integrity risk;

Ω_j denotes the set of particle indices associated with the j th vector containing fault indicators, such that the particles lie within AL of the mean state estimate \hat{x}_t ;

$w_t^{(i,j)}$ denotes the i th particle weight in the set of particles associated with j th multipath indicator vector at time t .

This formulation assumes that the combined distribution estimated by the particle filters in [27] accurately models the probabilities at tail-ends of the state probability distribution. However, such an assumption might not always hold, since the particle filter algorithm is designed to estimate the probability distribution near the most probable states and not the tail-ends [31]. Therefore, we propose an alternative approach to compute integrity risk directly from our GMM measurement likelihood,

$$P_I \approx \hat{P}_I = 1 - \int_{x \in \Omega_I} \sum_{k=1}^{K_t} \gamma_k \mathcal{N}(m_t^{(k)} | \rho_x^k, \sigma_x^k) dx, \quad (22)$$

where

Ω_I denotes the set of positions that lie within AL about the mean state estimate \hat{x}_t .

For computational efficiency, we approximate the above integral using cubature techniques for two-dimensional disks described in [43]. Note that our integrity risk computation is free from the probability distribution computed in the state estimation algorithm except in determining the confidence score γ_k parameters.

Accuracy is defined in [27] as the radius of the smallest disk about mean state estimate \hat{x}_t that contains the actual vehicle state with a prespecified probability α . Accuracy is determined mainly by the probability mass near the state estimate and not the tail-ends. First, we approximate the particle distribution by a Gaussian distribution with mean as mean state estimate \hat{x}_t , and covariance \mathbf{C} computed as a weighted estimate from samples as,

$$\mathbf{C} = \frac{1}{1 - \sum_{i=1}^N (w_t^{(i)})^2} \sum_{i=1}^N w_t^{(i)} (x_t^{(i)} - \hat{x}_t)(x_t^{(i)} - \hat{x}_t)^\top. \quad (23)$$

Next, we estimate the accuracy r_A using the inverse cumulative probability distribution of the approximated Gaussian distribution as,

$$r_A \approx \hat{r}_A = \max_{i=1,2} \sqrt{\mathbf{C}_{i,i}} \Phi^{-1}(\alpha) \quad (24)$$

where

\hat{r}_A is the estimated accuracy;

$\Phi^{-1}(\cdot)$ denotes the inverse cumulative probability function for standard Gaussian distribution.

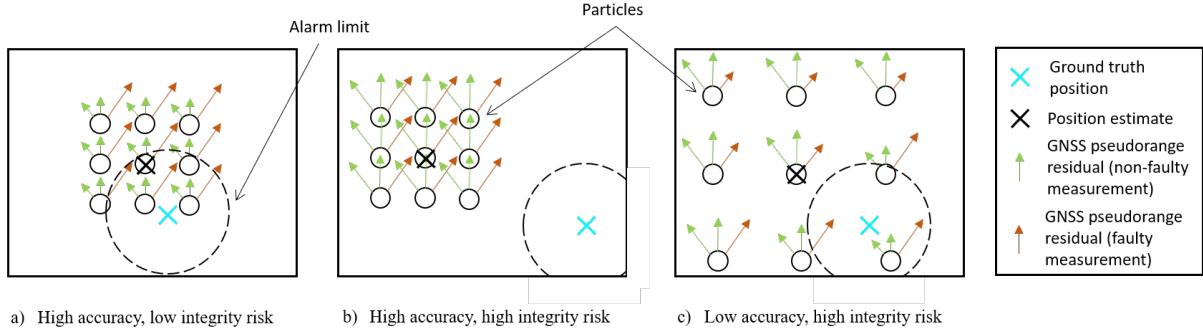


Figure 3: Three typical scenarios encountered by our integrity monitoring algorithm. Each scenario depicts one time instant with three GNSS pseudorange measurements. One out of the three measurements (orange) is contaminated with bias error, and the remaining two measurements (green) are non-faulty. In scenario a), state estimate is within alarm limit and the particles are close to each other (high accuracy, nominal operations). The residuals for non-faulty measurements (green) are smaller than the faulty measurement residuals (orange). Therefore, integrity risk is computed primarily from the GMM components of the non-faulty measurements (high confidence scores) and the system is declared available. In scenario b), state estimate is outside alarm limit and the particles are close to each other (high accuracy, hazardous operations). The residuals for all measurements are large. Therefore, integrity risk is computed from all GMM components (similar confidence scores) and the system is declared unavailable. In scenario c), state estimate is outside alarm limit and the particles are spread apart (low accuracy, hazardous operations). Different parts of the particle distribution have different measurement residuals. Therefore, integrity risk is computed from all GMM components (similar confidence scores) and the system is declared unavailable.

Availability is the probability that a positioning solution can be computed by the system with a required integrity risk P_I^0 and accuracy r_A^0 . We determine that our positioning system is available with probability 1 if,

$$(\hat{P}_I \leq P_I^0) \quad \text{and} \quad (\hat{r}_A \geq r_A^0). \quad (25)$$

If any of the above constraints are violated, the integrity monitoring algorithm declares the system unavailable.

Fig. 3 depicts three scenarios to explain the working of our integrity monitoring algorithm. In the first scenario, Particle RAIM correctly tracks the ground truth trajectory with high accuracy (nominal operations). Among the three measurements obtained for the current time instant, one measurement is contaminated with bias error. In such scenario, Particle RAIM correctly assigns high confidence scores to the non-faulty measurements and a low confidence score to the faulty measurement. Hence, a majority of the probability mass associated with the GMM measurement likelihood constructed from the measurements and confidence scores lies in the vicinity of the state estimate, resulting in small value of the integrity risk. Since the accuracy is high and the integrity risk is low, the integrity monitor correctly declares the system available. In the second scenario, Particle RAIM tracks an incorrect state with high accuracy (hazardous operations). Among the three measurements obtained at the current time instant, two measurements are non-faulty and the remaining third measurement contains a random bias error. In this case, Particle RAIM assigns similar confidence scores to the three measurements, since none of them support the particle distribution. Hence, the probability mass associated with the constructed GMM measurement likelihood lies away from the state estimate, resulting in a large value of the integrity risk. Since the integrity risk is high, the integrity monitor correctly declares the system unavailable. In the third scenario, the particle distribution in Particle RAIM is near the ground truth trajectory, but the particles are spread apart such that the computed accuracy is low (hazardous operations). The three measurements obtained at the current time instant support the positions in the vicinity of different particles. Again, Particle RAIM assigns similar confidence scores to the measurements, since each of them is supported by a different group of particles. Hence, the probability mass associated with the constructed GMM measurement likelihood is spread over a wide range of positions, resulting in a high value of the integrity risk. Since accuracy is low and integrity risk is high, the integrity monitor correctly declares the system unavailable. The third scenario can also result in false alarms by the integrity monitor if the position error in the state estimate computed from the particle distribution happens to be within the alarm limit.

F. Computation Time

Real-time performance and continuous operation are necessary aspects of a reliable navigation system. However, most existing algorithms based on RAIM or filter-bank approaches exhibit large computation overheads when more than a few (one or two) measurement faults are considered. For example, in solution-separation RAIM [5] and filter-bank approaches [44], different hypotheses associated with certain measurements being faulty need to be considered. For maximum m faults considered within k available measurements, the number of such hypotheses roughly grows on the order of $O(k^m)$.

Instead, Particle RAIM addresses multiple faults using a GMM-based voting scheme, that grows linearly in computation with the number of available measurements. For n particles and k available measurements, both the vote computation and vote pooling have a complexity of $O(nk)$. Constructing the GMM likelihood from confidence scores requires $O(k)$ computations. Finally, computing weights for each extended space particle requires $O(nk)$ computations. All these operations together exhibit a computational complexity of at most $O(nk)$, or linear in k for a fixed n . Furthermore, each of these steps admits parallelization. For example, all votes from particles to measurements can be computed in parallel and pooling of votes can be performed at the same time across different measurements. Additionally, weights for all the particles can be computed simultaneously from the likelihood model, resulting in further speedups. However, the number of particles required to adequately approximate the probability distribution increase exponentially with the size of the state-space [20]. In order to maintain a small computation cost with large state-spaces, more complex strategies, such as Rao-Blackwellization [45] or leveraging prior knowledge about probability distribution, need to be employed.

III. Experimentation Results

We evaluated the framework for localization performance and integrity monitoring on both simulated as well as real-world data. For the experiments on simulated data, we validate our algorithm across multiple runs on various simulated noise profiles that imitate GNSS measurements in urban environments. All the filters are initialized at the ground truth initial position with a specified standard deviation σ_{init} . Note that for Particle RAIM, we only use a single iteration in the weighting step in our experiments on simulated data, since we observed that a single iteration suffices to provide us good performance at low computation cost.

We consider two baselines to compare against our Particle RAIM algorithm:

Joint state-space particle filter (J-PF) For our first baseline, we consider the particle filter algorithm proposed by Pesonen [27] which considers both the vehicle navigation parameters and measurement fault vector (signal quality parameters) in the particle filter state-space. The combined state-space is referred to as the *joint state-space*. J-PF requires considering separate particles for each binary-valued vector denoting faulty measurements, resulting in a combinatorial growth in computational complexity on increasing number of considered faults. For example, when only 1 fault is considered in 10 available measurements, the different sets of particles considered by the algorithm is 10, each associated with the fault being present in one of the 10 measurements. When the number of faults is increased to 2, all the pairs of measurements need to be considered increasing the number of particle sets to 55 (both single and double faults). With 3 faults, this number becomes 175. Therefore, we limit the number of faults considered in GNSS measurements for J-PF to at most 2 for computational tractability. The particle filter approach described in [27] also assumes a transition model for fault indicators across time instants. To compare against our approach which does not assume a transition model for fault indicators, we set the fault indicator transitions in J-PF to be equally probable from the most likely (highest log likelihood) fault indicator vector at the current time instant to any other vector. For all the fault indicator vectors that are not the most likely, we set the transitions to any other vector as zero. This approach is also in line with the Rao-Blackwellized particle filter discussed in the same paper [27] as well as filter bank approaches [44], where the filter distribution with the highest log-likelihood is selected to represent the probability distribution at a time instant. However, we only use the highest log-likelihood probability distribution for transitions and computation of state estimate. The parameters for integrity monitoring are computed using all the particles.

Parameter	Value
# of satellites	5-10
GNSS ranging noise σ_{GNSS}	5-10 m
GNSS ranging bias error magnitude	50-200 m
Maximum # of faulty measurements	1-6
GNSS fault change probability	0.2
Vehicle speed	10 m/s
Odometry noise σ_u	5 m/s
# of particles	200
Filter initialization σ_{init}	5 m
Filter measurement model noise $\{\sigma^k\}_{k=1}^K$	5 m
Filter propagation model noise σ_f	5 m

Table 2: Table of experiment parameters for simulated scenario

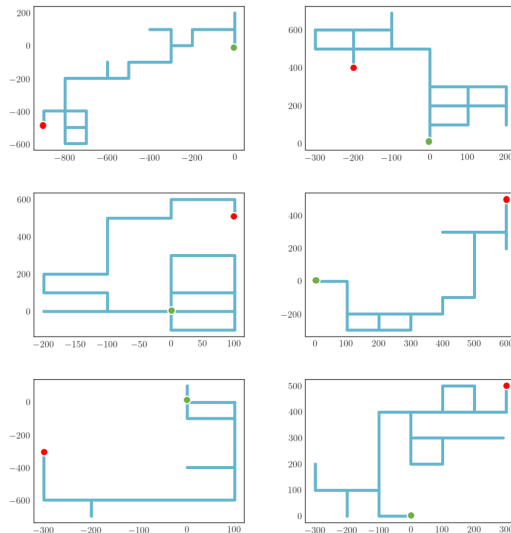


Figure 4: Sample trajectories (cyan) from randomly generated simulation dataset. The start and end points of the trajectories are drawn in green and red respectively. Each trajectory is approximately 4000 m long and of duration 400 s.

Kalman filter RAIM (KF-RAIM) Our second baseline is based on the Kalman filter RAIM algorithm with multiple measurement fault detection and exclusion [9]. The measurement faults are detected using the chi-square test statistic computed from the Kalman filter mean state estimate. We iteratively exclude the measurement with the largest residual and perform the Kalman filter measurement update till the test statistic falls below a prespecified threshold. Integrity in KF-RAIM is monitored using the sequence of normalized Kalman filter innovations [17] with a window size of 10 time instants.

We discuss our experimental results in 5 parts: (A) evaluation of Particle RAIM localization performance on simulated data and comparison with KF-RAIM and J-PF approaches, (B) evaluation of Particle RAIM on real-world data, (C) comparison of our integrity monitoring technique with [27] in terms of probability of false alarm and probability of missed-identification on simulated scenarios, (D) analysis of the computation time of our algorithm and comparison in terms of computation with KF-RAIM and J-PF approaches, and (E) discussion of the results.

A. Evaluation on simulated data

An advantage of using simulations is that we can evaluate the Particle RAIM approach under changing environments with varying noise values and differing number of faulty measurements, which are hard to ensure when collecting real world data. Furthermore, the ground truth of vehicle’s position is available in simulations as opposed to in real-world scenarios. We construct the simulated environment in Python programming language to test our algorithm. In the environment, simulated satellites move along well-separated predefined paths at fixed heights from the surface. The environment includes a vehicle moving on the horizontal surface according to 50 different randomly generated trajectories approximately of length 4000 m each (Fig. 4). The motion of the agent lasts for 400 s with measurements acquired at the rate of 1 Hz. The vehicle obtains noisy GNSS ranging measurements from the satellites as well as noisy odometry measurements. The parameters used for the simulation and filter are given in Table 2.

We induce two kinds of noise profiles in our pseudorange measurements from the simulation - a zero mean Gaussian random noise on all measurements and a random bias noise on a subset of measurements. The subset of measurements containing the bias noise is initialized randomly, and henceforth has a small probability of changing to a different random subset at every subsequent time instant. The maximum number of measurements affected is selected randomly at every change, and the minimum is kept zero. The zero mean Gaussian noise is applied to

		Few-fault scenarios			Many-fault scenarios		
		(5, 1)	(5, 2)	(7, 3)	(7, 4)	(10, 5)	(10, 6)
KF-RAIM	RMSE(m)	7.57	21.52	21.93	34.28	25.52	34.42
	%>15 m	5.88	68.72	69.64	87.37	80.53	91.10
J-PF	RMSE(m)	4.86	5.77	28.09	33.48	25.65	22.92
	%>15 m	1.22	3.10	79.01	94.22	68.27	85.45
Particle RAIM	RMSE(m)	11.06	12.39	11.73	13.21	12.20	12.37
	%>15 m	23.42	26.60	27.44	33.06	24.29	28.70

Table 3: Comparison of localization performance on the simulated dataset. The dataset consists of varying total number of measurements and maximum number of measurement faults (total # of measurements, max # of faults). Particle RAIM demonstrates better localization performance in scenarios with large number of faults in comparison to J-PF and KF-RAIM.

measurements such that the variance is double the normal value for biased measurements. Using our noise model, we simulate the effects of NLOS signals and multipath on pseudorange measurements in urban GNSS navigation. The state-space for all algorithms consists of the 2D state (x, y) of the vehicle moving on a horizontal surface. We limit the state estimation to a simple case for simulations in view of the computational overhead from requiring a larger number of particles.

Localization performance In this experiment, we consider different numbers of GNSS measurements available at a time instant, as well as different maximum numbers of faulty measurements. We compare the localization performance of our Particle RAIM algorithm with that of J-PF and SR-RAIM approaches. We consider the following scenarios (total # of measurements, max # of faults): (5, 1), (5, 2), (7, 3), (7, 4), (10, 5), (10, 6). For each of these scenarios, we use the bias value of 100 m as well as GNSS measurement standard deviation of 10 m. We compute the metrics of horizontal root mean square error (RMSE) as well as percentage of estimates that are more than 15 m away from ground truth (%>15 m). All of the metrics have been computed from 50 full runs roughly of length 4000 m each across different randomly generated trajectories.

The trajectories for two scenarios, (5, 1) and (10, 5), are visualized for each algorithm in Fig. 5 and the computed metrics are recorded in Table 3. As can be seen from the qualitative and quantitative results, Particle RAIM demonstrates better localization performance than the compared approaches for scenarios with high noise degradation while maintaining a low rate of large positioning errors. J-PF has better performance than its counterparts in scenarios with single faults due to considering all possibilities of faults explicitly. However, its performance considerably worsens when the number of faults in measurements exceed the number of faults considered in the filter, which needs to be a small number to ensure computational tractability. For scenarios with a low fraction of faulty measurements, KF-RAIM is able to identify and remove faults resulting in lower positioning errors. However, KF-RAIM demonstrates poor performance in scenarios with a high fraction of faulty measurements, which is expected since it only incorporates sequential information from previous time instants and odometry in initialization, unlike Particle RAIM and J-PF.

Varying GNSS measurement noise In this experiment, we study the impact of GNSS measurement noise bias and standard deviation values on the performance of our algorithm. First, keeping the GNSS measurement standard deviation fixed at 5 m, we vary the bias between 10 – 100 m in increments of 10 m. Next, keeping the bias fixed at 100 m, we vary the standard deviation between 5 – 25 m in increments of 5 m. For all cases, the total number of measurements is kept at 7 and the maximum number of faults is 3. The RMSE for both studies are computed across 20 different runs and plotted in Fig. 6.

The first plot shows that the localization performance of Particle RAIM initially deteriorates and then starts improving. This is because for low bias error values, the faulty GNSS measurements do not have a significant impact

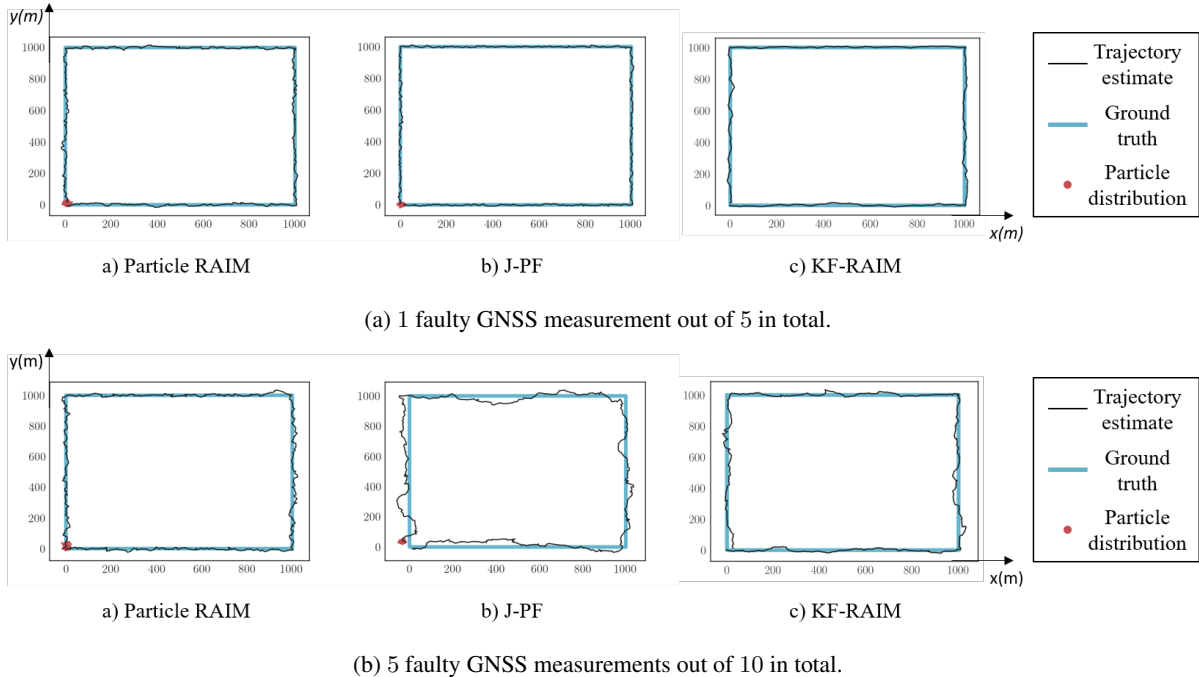


Figure 5: Localization accuracy comparison between Particle RAIM, J-PF, and KF-RAIM approaches for (a) few-fault scenario and (b) many-fault scenario. We fix the underlying ground truth trajectory to be a square of side 1000 m with $(0, 0)$ as both the start and end positions. Unlike J-PF and KF-RAIM, Particle RAIM is able to estimate the vehicle state with good accuracy in scenarios with a large fraction of faulty measurements.

on the localization solution, even if the algorithm fails to remove them. Beyond the bias error value of 50 m, the algorithm successfully assigns lower confidence scores to faulty measurements, resulting in lower RMSE for higher bias error values. The second plot demonstrates the impact of high measurement noise standard deviation on our approach. As the measurement noise standard deviation is increased, the RMSE increases in a superlinear fashion. The performance deteriorates with increasing noise standard deviation since both the tasks of fault mitigation as well as localization are negatively impacted by an increased measurement noise.

Another key parameter for performance in Particle RAIM is the number of particles. Similar to the other particle filter algorithms, the number of particles required to approximate the posterior probability distribution at a time instant depends on the precision required in localization as well as on the size of the state space. Since the precision in localization is also limited by the precision of measurements used in Particle RAIM, there is no significant improvement in the algorithm performance on the simulation scenarios on increasing the number of particles beyond 100. On increasing the size of the state space, the number of particles required to approximate the posterior probability distribution increases exponentially [20].

B. Evaluation on real-world data

For the real-world case, we use GNSS pseudorange and odometry measurements from the publicly available urban GNSS dataset collected by TU Chemnitz for project smartLoc [46]. The dataset was collected on a vehicle moving in urban environments, using a low-cost u-blox EVK-M8T GNSS receiver at 5 Hz and CAN data for odometry at 50 Hz. The odometry data contains both speed and heading information from an onboard magnetometer. The ground truth or reference position is provided using a high-cost NovAtel GNSS receiver at 20 Hz. Additionally, corrections to satellite ephemeris data are also provided as an SP3 file along with the data. We consider Frankfurt Westend-Tower trajectory from the TU-Chemnitz GNSS dataset [46] for evaluating our approach. The trajectory is roughly 2300 m long and has both dense and sparse urban regions, with 32% measurements being NLOS signals on average. The GNSS measurements consist of signals from GPS, GLONASS, and Galileo satellite constellations with roughly 12 measurements being available on average at each time instant. As a preprocessing step, we remove the clock error differences between measurements from different constellations as well as assign

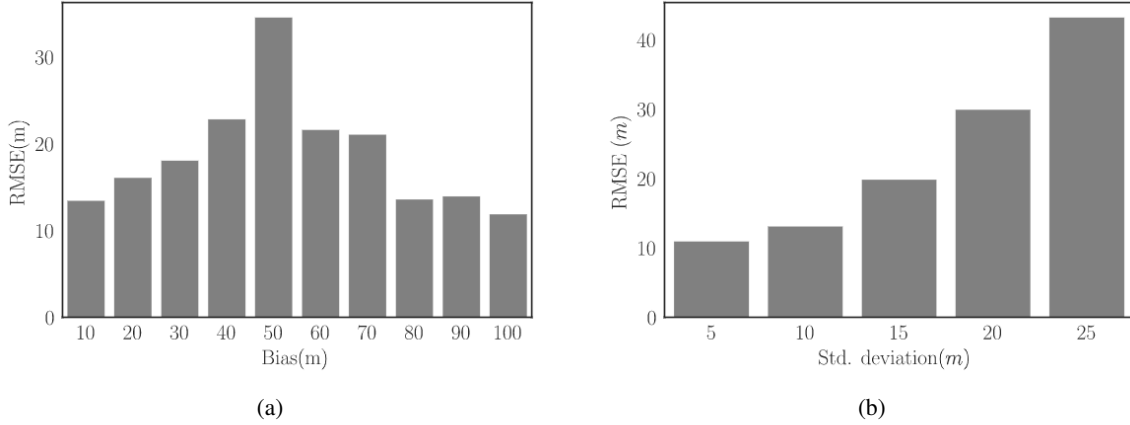


Figure 6: Sensitivity analysis of Particle RAIM localization performance with varying values of GNSS measurements (a) bias and (b) standard deviation. For low values of bias, the faults do not significantly impact the navigation solution, resulting in low RMSE values. Beyond the value of 50 m, Particle RAIM is able to remove the impact of faulty measurements resulting in low RMSE values. The performance of the algorithm increasingly deteriorates with higher standard deviation in GNSS measurement noise since both the capability to remove faulty measurements as well as localization are hampered by an increased noise.

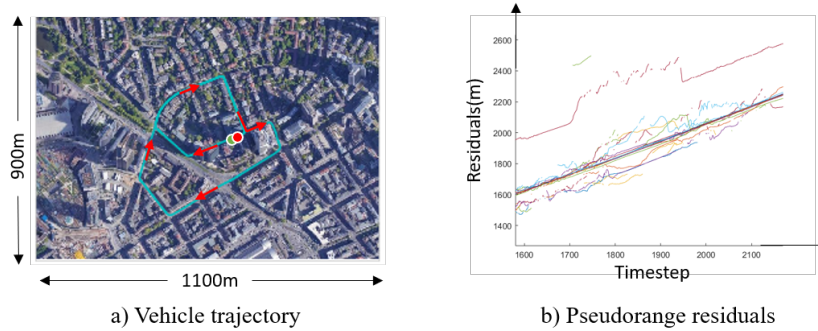


Figure 7: Real-world dataset for validation of our approach. We use Frankfurt Westend-Tower sequence from smartLoc project dataset collected by TU Chemnitz [46]. The trajectory followed by the vehicle is shown in a). The vehicle moves from the start point (green) to end point (red) along the trajectory (cyan) in the direction specified by red arrows. b) shows a plot of pseudorange measurement residuals from different satellites with respect to ground truth position from part of the dataset for a duration of 2 minutes. The residuals were corrected for clock differences across different GNSS constellations. Multiple pseudorange measurement residuals demonstrate errors due to multipath effects in the urban environment.

zero residuals to all GNSS measurements at the initial vehicle position, by subtracting the measurement residuals corresponding to the initial vehicle state from all measurements. Fig. 7 shows the reference trajectory used for evaluation as well as measurement residuals with respect to ground truth position for a duration of 2 minutes.

For state estimation using Particle RAIM, KF-RAIM, and J-PF on the Frankfurt dataset, our state-space consists of the vehicle position (x, y) , heading θ , and clock bias error δt . To mitigate the impact of clock drift, we denote clock bias error δt as the difference between the true receiver clock bias and a simple linear drift model with precomputed drift rate, and estimate this difference across time instants in each of the algorithms. For Particle RAIM and J-PF, we use 1000 particles to account for a larger state space size than the simulated scenario.

Fig. 8 shows a comparison between position estimates from Particle RAIM, J-PF, and KF-RAIM. Particle RAIM position estimates with 5 iterations within the algorithm are closer to the ground truth than compared approaches and have lower horizontal RMSE values. Furthermore, the trajectory estimated using Particle RAIM is smoother,

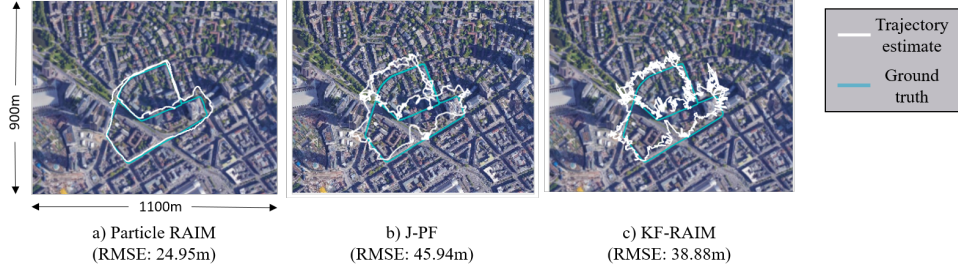


Figure 8: Estimated trajectories on real-world data. Positions estimated using Particle RAIM (5 iterations) (a) are closer to ground truth as compared to estimation using J-PF (b) and KF-RAIM (c). The horizontal RMSE values are computed by averaging over 20 runs with different randomness values in initialization and propagation. In regions with multiple measurements contaminated with bias errors, Particle RAIM (a) is able to localize correctly by assigning high confidence scores to measurements that are consistent with the particle filter probability distribution of vehicle state.

since it leverages the particle filter probability distribution of state to remove erroneous GNSS measurements.

C. Comparison of integrity monitoring approaches

We study the integrity monitoring performance of Particle RAIM on simulated and real-world data. Since obtaining a large amount of real-world data is difficult and out of scope for this work, we restrict our numerical analysis to simulated data and only provide qualitative results on real-world data. For the simulated scenario, we generate 400 s long trajectories with GNSS pseudorange measurements acquired at the rate of 1 Hz (Fig. 9 a)). GNSS pseudorange measurements are simulated from 10 different satellites. At time instants between 125-175 s and 225-275 s, we add bias errors in upto 60% of the available measurements, such that the faulty measurements correspond to a position offset from the ground truth position. The position offset is randomly selected across different runs from between 50 – 150 m. To limit our analysis to GNSS measurements, we do not simulate any odometry measurements for the simulations and localize only using GNSS pseudorange measurements for all the filters. For the particle filter algorithms, we set the propagation noise standard deviation to 20 m to ensure that the position can be tracked in the absence of odometry measurements.

We compare our integrity monitoring approach with the Bayesian RAIM method described in [27] using J-PF for state estimation, and the Kalman innovation sequence method described in [17] using KF-RAIM for state estimation. The system is declared to be in hazardous operations when the positioning error in the navigation system exceeds an alarm limit, which we set to 20 m. The approaches are evaluated on the metrics of estimated probability of false alarm $\hat{P}(FA)$ and probability of missed-identification $\hat{P}(MI)$. Each of these metrics are computed as,

$$\hat{P}(FA) = \frac{N(I_{av} \cap \neg I_{ho})}{N(\neg I_{ho})}, \quad (26)$$

$$\hat{P}(MI) = \frac{N(\neg I_{av} \cap I_{ho})}{N(I_{ho})}, \quad (27)$$

where

$N(\cdot)$ denotes number of occurrences of an event;

$I_{av}(\neg I_{av})$ denotes the event when the navigation system is declared available (unavailable) by the integrity monitoring algorithm;

$I_{ho}(\neg I_{ho})$ denotes the event of hazardous operations (normal operations);

T denotes the total number of timesteps for which the algorithm is run.

The integrity monitoring algorithms in all 3 considered approaches depend on different threshold values, such as minimum accuracy and integrity risk for Particle RAIM and Bayesian RAIM and the threshold for the innovation-based statistic in KF-RAIM. Therefore, we compare these approaches by plotting the probability of false alarm

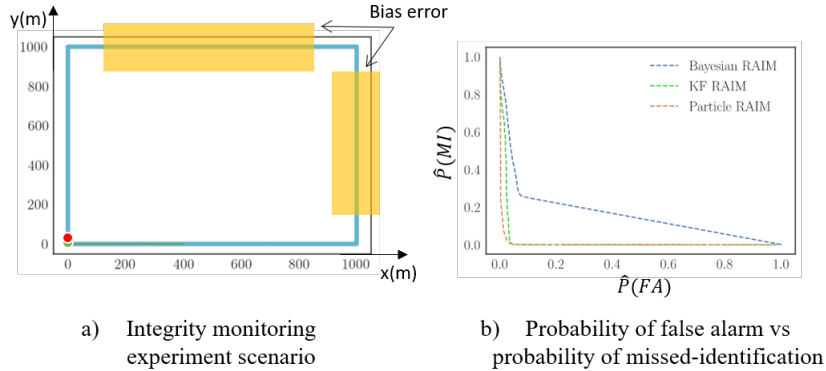


Figure 9: (a) Simulation experiment scenario for analyzing integrity monitoring performance. The start and end of the 400 s long trajectory are marked in green and red, respectively. The yellow regions denote the 125 – 175 s and 225 – 275 s positions in the trajectory, when bias errors are induced in upto 60% of the total 10 simulated GNSS measurements. (b) Probability of false alarms and probability of missed-identifications across different integrity monitoring threshold values for Particle RAIM, Bayesian RAIM [27], and innovation sequence in KF RAIM [17]. Particle RAIM generates the least false alarms and missed-identifications among the compared approaches on the simulated scenario, closely followed by KF-RAIM.

and probability of missed-identification metrics for the different algorithms across different values of the thresholds (Fig. 9 b)). All the metrics are calculated using more than 10^4 samples across multiple runs of the simulation for each algorithm. Fig. 9 b) shows that Particle RAIM generates the least false alarms and missed-identifications among the compared approaches on the simulated scenario, closely followed by KF-RAIM.

For qualitative analysis of the real-world performance of the technique, a plot of RMSE and Particle RAIM system fault detections using real-world data is presented in Fig. 10. The integrity risk and accuracy thresholds for the scenario are chosen to minimize missed-identifications while maintaining high availability. As can be seen in the figure, Particle RAIM declares the system unavailable in most of the cases when positioning error exceeds the alarm limit.

The number of particles used in Particle RAIM is an important parameter to analyze for studying the integrity monitoring performance. As the number of particles used for approximating the posterior probability distribution in the filter is increased, a decrease in the variance of the estimates of both integrity risk and accuracy is observed. However, since the system availability depends on thresholding the estimates of integrity risk and accuracy, we do not observe a significant decrease in the probability of false alarm and probability of missed-identification when a large number of particles is used.

D. Analysis of computation time

We compare the computational performance of our Particle RAIM algorithm with J-PF and KF-RAIM approaches. The average time per timestep in milliseconds is shown in Fig. 11. For Particle RAIM and J-PF approaches, we consider 1000 particles in the particle filter. In Particle RAIM, we apply a single iteration for computing confidence scores. The methods are compared for a scenario with 10 total measurements and 6 faults. Particle RAIM requires less than half of the computation time required by J-PF, which only considers upto 2 faults. KF-RAIM exhibits the least computation time since the updates are calculated analytically instead of using particles. Table 4 contains the fractions of total computation time taken up by different components of the Particle RAIM algorithm. The maximum fraction of the computation time is taken by the RAIM voting and mixture weighting steps, since they require accessing each particle as well as measurement and performing multiple operations on them. The benchmarking is done on a laptop computer with Intel i7-9750H x64-based processor with 16 Gigabytes of RAM and a 6 core 2.60 GHz CPU.

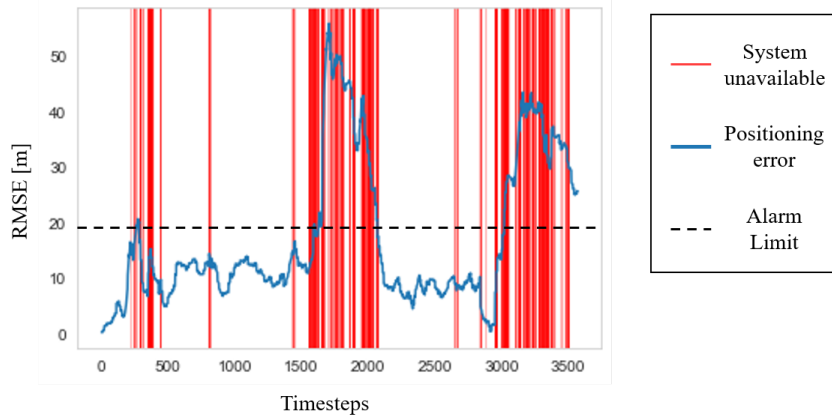


Figure 10: Particle RAIM system availability on real-world data. Our integrity monitoring algorithm is able to detect most system faults when positioning error exceeds the alarm limit.

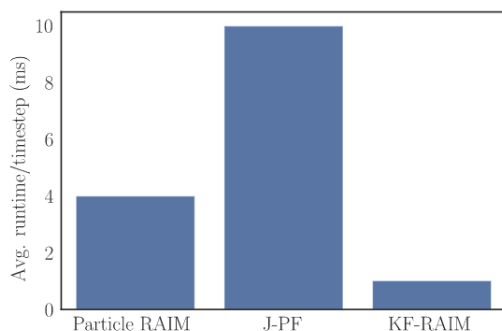


Figure 11: Comparison of computation times in Particle RAIM, J-PF and KF-RAIM. Particle RAIM exhibits lower computation time than J-PF due to its linear-time complexity algorithm. KF-RAIM exhibits the least computation time since the updates are calculated analytically instead of using particles.

Component	Compute[%]
Propagation	0.35
Measurement voting	49.55
Vote pooling	0.29
Mixture weighting	49.28
Resampling	0.53

Table 4: Component-wise fractions of total computation time in Particle RAIM. Measurement voting and Mixture weighting are the most computation-heavy components in the algorithm, since they involve multiple operations across all particles and measurements.

E. Discussion

The performance evaluations on both simulated and real-world data for state estimation show that Particle RAIM achieves lower state estimation errors as compared to J-PF and KF-RAIM approaches. Furthermore, evaluation of the integrity monitoring technique on simulated data shows that compared to Bayesian RAIM and Kalman filter innovation sequence based techniques, Particle RAIM demonstrates lower probability of false alarm and probability of missed-identification in determining system availability. A study of the computational performance shows that Particle RAIM is faster than existing particle filter-based approaches that use banks of filters, and therefore can be deployed in real-time scenarios with multiple measurements contaminated with bias errors at each time instant.

Although Particle RAIM achieves good localization performance in simulated scenarios with multiple faulty measurements, the algorithm’s performance in scenarios with one or two measurement faults is worse than J-PF. This is because the algorithm is designed with conservative choices, such as the GMM measurement likelihood model instead of the commonly used multivariate Gaussian model. Another limitation of our approach is that the fault mitigation strategy in Particle RAIM uses the predicted probability distribution from the previous timestep which is approximated using particles. Therefore, in scenarios where the probability distribution tracked by the parti-

cles significantly differs from the true posterior probability distribution at the previous time instant, the algorithm might compute incorrect confidence scores that might cause the filter to diverge in extreme scenarios. Resetting strategies for the filter might help in maintaining good performance in such scenarios. However, analysis of such techniques is out of scope for this paper and left as an avenue for future research.

The integrity monitoring algorithm proposed in this paper is also based on conservative decision choices, such as computing the integrity risk by numerically integrating the GMM measurement likelihood. Hence, the algorithm often generates false alarms even when the filter state estimate is close to the ground truth. Considering measurement likelihood models other than the GMM likelihood which are less conservative can therefore be another avenue for future research.

Although the results of our analysis of Particle RAIM using simulated and real-world data are promising, the performance of the algorithm solely based on GNSS pseudorange and odometry measurements is insufficient for providing precise localization and ensuring safety in urban environments. Therefore, an important future direction is to explore additional sensor modalities for precise navigation, such as carrier phase measurements. In theory, higher precision in localization coupled with larger number of particles additionally improves the performance of the integrity monitor, since integrity risk and accuracy can be computed more precisely for smaller alarm limits.

IV. Conclusion

In this paper, we presented Particle RAIM as a novel probabilistic framework for robust localization and integrity monitoring in challenging urban environments. Particle RAIM leverages GNSS and odometry measurements to compute a fault-robust probability distribution of the vehicle position and generates warnings if a reliable position cannot be estimated. We represent the state probability distribution at a time instant using weighted particles in a particle filter. Then, we use odometry measurements to propagate the particles to the subsequent time instant. To update the weights of all particles using GNSS measurements in a fault-robust manner, we developed a measurement likelihood model based on GMM and determine the GMM weight coefficients at runtime. Each component in our GMM likelihood represents the probability of observing a single GNSS measurement from a position. Using an iterative approach based on the EM algorithm, we estimate the weight coefficients in the GMM likelihood jointly with the particle filter weights. To monitor the state estimation system's integrity and generate timely warnings, we then compute measures of integrity risk as well as accuracy and compare them against prespecified requirements. Through a series of experiments on simulated and real-world data, we have shown that Particle RAIM achieves lower positioning errors in state estimation as well as lower probability of false alarm and probability of missed-identification in integrity monitoring as compared with existing approaches in challenging urban environments. Furthermore, the computation time requirement of the iterative fault mitigation approach in Particle RAIM is significantly lower than that of existing particle filter-based approaches which consider multiple subsets of GNSS measurements. These results enable Particle RAIM to be a useful direction for future research on developing high-integrity algorithms for urban environments that can be deployed in real-time.

Acknowledgements

This material is based upon work supported by the National Science Foundation under award #2006162.

References

- [1] N. Zhu, J. Marais, D. Bétaille, and M. Berbineau, "GNSS position integrity in urban environments: A review of literature," *IEEE Transactions on Intelligent Transportation Systems*, vol. 19, no. 9, pp. 2762–2778, 2018.
- [2] S. Pullen, T. Walter, and P. Enge, "Sbas and gbas integrity for non-aviation users: Moving away from" specific risk,"
- [3] B. W. Parkinson, P. Enge, P. Axelrad, and J. J. Spilker Jr, *Global positioning system: Theory and applications, Volume II*. American Institute of Aeronautics and Astronautics, 1996.
- [4] M. Joerger, F.-C. Chan, and B. Pervan, "Solution separation versus residual-based RAIM," *NAVIGATION: Journal of the Institute of Navigation*, vol. 61, no. 4, pp. 273–291, 2014.
- [5] R. G. Brown and P. W. McBurney, "Self-Contained GPS Integrity Check Using Maximum Solution Separation," *Navigation*, vol. 35, no. 1, pp. 41–53, 1988.
- [6] Y. C. Lee *et al.*, "Analysis of range and position comparison methods as a means to provide GPS integrity in the user receiver," in *Proceedings of the 42nd Annual Meeting of the Institute of Navigation*, pp. 1–4, Citeseer, 1986.

- [7] M. Joerger and B. Pervan, "Solution separation and Chi-Squared ARAIM for fault detection and exclusion," in *2014 IEEE/ION Position, Location and Navigation Symposium-PLANS 2014*, pp. 294–307, IEEE, 2014.
- [8] J. Blanch, K. Gunning, T. Walter, L. De Groot, and L. Norman, "Reducing computational load in solution separation for kalman filters and an application to ppp integrity," in *Proceedings of the 2019 International Technical Meeting of The Institute of Navigation*, pp. 720–729, 2019.
- [9] B. W. Parkinson and P. Axelrad, "Autonomous GPS integrity monitoring using the pseudorange residual," *Navigation*, vol. 35, no. 2, pp. 255–274, 1988.
- [10] M. A. Sturza, "Navigation system integrity monitoring using redundant measurements," *Navigation*, vol. 35, no. 4, pp. 483–501, 1988.
- [11] M. Joerger and B. Pervan, "Sequential residual-based raim," in *Proceedings of the 23rd international technical meeting of the satellite division of the institute of navigation (ION GNSS 2010)*, pp. 3167–3180, 2010.
- [12] J. Blanch, T. Walter, P. Enge, Y. Lee, B. Pervan, M. Rippl, and A. Spletter, "Advanced RAIM user algorithm description: integrity support message processing, fault detection, exclusion, and protection level calculation," in *Proceedings of the 25th International Technical Meeting of The Satellite Division of the Institute of Navigation (ION GNSS 2012)*, pp. 2828–2849, 2012.
- [13] S. Wallner, "A Proposal for Multi-Constellation Advanced RAIM for Vertical Guidance."
- [14] A. Grosch, O. G. Crespillo, I. Martini, and C. Günther, "Snapshot residual and Kalman filter based fault detection and exclusion schemes for robust railway navigation," in *2017 European Navigation Conference (ENC)*, pp. 36–47, IEEE, 2017.
- [15] S. Hewitson and J. Wang, "Extended receiver autonomous integrity monitoring (e raim) for gnss/ins integration," *Journal of Surveying Engineering*, vol. 136, no. 1, pp. 13–22, 2010.
- [16] Z. Li, D. Song, F. Niu, and C. Xu, "RAIM algorithm based on robust extended Kalman particle filter and smoothed residual," in *China Satellite Navigation Conference*, pp. 209–220, Springer, 2017.
- [17] C. Tanil, S. Khanafseh, M. Joerger, and B. Pervan, "Sequential integrity monitoring for kalman filter innovations-based detectors," in *Proceedings of the 31st International Technical Meeting of the Satellite Division of The Institute of Navigation (ION GNSS+ 2018)*, pp. 2440–2455, 2018.
- [18] C. Boucher, A. Lahrech, and J.-C. Noyer, "Non-linear filtering for land vehicle navigation with gps outage," in *2004 IEEE International Conference on Systems, Man and Cybernetics (IEEE Cat. No. 04CH37583)*, vol. 2, pp. 1321–1325, IEEE, 2004.
- [19] W. Ershen, Z. Shufang, and H. Qing, "Research on gps receiver autonomous integrity monitoring algorithm based on mcmc particle filtering [j]," *Chinese Journal of Scientific Instrument*, vol. 10, 2009.
- [20] A. Doucet and A. M. Johansen, "A tutorial on particle filtering and smoothing: Fifteen years later," *Handbook of nonlinear filtering*, vol. 12, no. 656-704, p. 3, 2009.
- [21] J. Ahn, D. H. Won, Y. J. Lee, G. W. Nam, M.-B. Heo, S. Sung, *et al.*, "Gps integrity monitoring method using auxiliary nonlinear filters with log likelihood ratio test approach," *Journal of Electrical Engineering & Technology*, vol. 6, no. 4, pp. 563–572, 2011.
- [22] E. Wang, T. Pang, M. Cai, and Z. Zhang, "Fault Detection and Isolation for GPS RAIM Based on Genetic Resampling Particle Filter Approach," *TELKOMNIKA Indones. J. Electr. Eng.*, vol. 12, no. 5, pp. 3911–3919, 2014.
- [23] E. Wang, C. Jia, G. Tong, P. Qu, X. Lan, and T. Pang, "Fault detection and isolation in GPS receiver autonomous integrity monitoring based on chaos particle swarm optimization-particle filter algorithm," *Adv. Sp. Res.*, 2018.
- [24] L.-T. Hsu, Y. Gu, and S. Kamijo, "NLOS correction/exclusion for GNSS measurement using RAIM and city building models," *Sensors*, vol. 15, no. 7, pp. 17329–17349, 2015.
- [25] S. Miura, S. Hisaka, and S. Kamijo, "Gps multipath detection and rectification using 3d maps," in *16th International IEEE Conference on Intelligent Transportation Systems (ITSC 2013)*, pp. 1528–1534, IEEE, 2013.
- [26] L.-T. Hsu, F. Chen, and S. Kamijo, "Evaluation of multi-gnss and gps with 3d map methods for pedestrian positioning in an urban canyon environment," *IEICE Transactions on Fundamentals of Electronics, Communications and Computer Sciences*, vol. 98, no. 1, pp. 284–293, 2015.
- [27] H. Pesonen, "A framework for bayesian receiver autonomous integrity monitoring in urban navigation," *Navigation*, vol. 58, no. 3, pp. 229–240, 2011.
- [28] S. Gupta and G. X. Gao, "Particle RAIM for Integrity Monitoring," in *ION GNSS+*, 2019.
- [29] D. Geary, "Mixture models: Inference and applications to clustering," *Journal of the Royal Statistical Society Series A*, vol. 152, no. 1, pp. 126–127, 1989.
- [30] A. P. Dempster, N. M. Laird, and D. B. Rubin, "Maximum likelihood from incomplete data via the EM algorithm," *Journal of the Royal Statistical Society: Series B (Methodological)*, vol. 39, no. 1, pp. 1–22, 1977.
- [31] R. Van Der Merwe, A. Doucet, N. De Freitas, and E. A. Wan, "The unscented particle filter," in *Advances in neural information processing systems*, pp. 584–590, 2001.
- [32] M. K. Simon, *Probability distributions involving Gaussian random variables: A handbook for engineers and scientists*. Springer Science & Business Media, 2007.
- [33] P. A. M. Dirac, *The principles of quantum mechanics*. No. 27, Oxford university press, 1981.
- [34] Z. Chen *et al.*, "Bayesian filtering: From kalman filters to particle filters, and beyond," *Statistics*, vol. 182, no. 1, pp. 1–69, 2003.
- [35] M. Joerger and B. Pervan, "Kalman filter-based integrity monitoring against sensor faults," *Journal of Guidance, Control, and Dynamics*, vol. 36, no. 2, pp. 349–361, 2013.
- [36] L. Yu, "Research on GPS RAIM Algorithm Based on SIR Particle Filtering State Estimation and Smoothed Residual," *Appl. Mech. Mater.*, vol. 422, pp. 196–203, 2013.
- [37] X. Zhao, Y. Qian, M. Zhang, J. Niu, and Y. Kou, "An improved adaptive Kalman filtering algorithm for advanced robot navigation system based on GPS/INS," in *2011 IEEE International Conference on Mechatronics and Automation*, pp. 1039–1044, IEEE, 2011.
- [38] J. P. Vila and P. Schniter, "Expectation-maximization Gaussian-mixture approximate message passing," *IEEE Transactions on Signal Processing*, vol. 61, no. 19, pp. 4658–4672, 2013.
- [39] C. M. Bishop, *Pattern recognition and machine learning*. springer, 2006.
- [40] F. Gustafsson, F. Gunnarsson, N. Bergman, U. Forssell, J. Jansson, R. Karlsson, and P.-J. Nordlund, "Particle filters for positioning, navigation, and tracking," *IEEE Transactions on signal processing*, vol. 50, no. 2, pp. 425–437, 2002.
- [41] J. Cho, "On the enhanced detectability of GPS anomalous behavior with relative entropy," *Acta Astronautica*, vol. 127, pp. 526–532, 2016.
- [42] M. Tossaint, J. Samson, F. Toran, J. Ventura-Traveset, M. Hernández-Pajares, J. Juan, J. Sanz, and P. Ramos-Bosch, "The stanford-esa

- integrity diagram: A new tool for the user domain sbas integrity assessment,” *Navigation*, vol. 54, no. 2, pp. 153–162, 2007.
- [43] F. G. Lether, “A generalized product rule for the circle,” *SIAM Journal on Numerical Analysis*, vol. 8, no. 2, pp. 249–253, 1971.
- [44] T. L. Lai, “Sequential multiple hypothesis testing and efficient fault detection-isolation in stochastic systems,” *IEEE Transactions on Information Theory*, vol. 46, no. 2, pp. 595–608, 2000.
- [45] A. Doucet, S. Godsill, and C. Andrieu, “On sequential Monte Carlo sampling methods for Bayesian filtering,” *Statistics and computing*, vol. 10, no. 3, pp. 197–208, 2000.
- [46] P. Reisdorf, T. Pfeifer, J. Breßler, S. Bauer, P. Weissig, S. Lange, G. Wanielik, and P. Protzel, “The problem of comparable gnss results—an approach for a uniform dataset with low-cost and reference data,” in *Proc. of Intl. Conf. on Advances in Vehicular Systems, Technologies and Applications (VEHICULAR)*, 2016.